Contrib Mineral Petrol (1999) 134: 3–16

Samuel A. Bowring · Ian S. Williams

Priscoan (4.00–4.03 Ga) orthogneisses from northwestern Canada

Received: 28 February 1997 / Accepted: 9 July 1998

Abstract Ancient crustal rocks provide the only direct evidence for the processes and products of early Earth differentiation. SHRIMP zircon U-Th-Pb dating has identified, amongst the Acasta gneisses of the western Slave Province, Canada, two metatonalites and a metagranodiorite that have igneous ages of 4002 ± 4, 4012 ± 6 and 4031 ± 3 Ga respectively. These are the first identified Priscoan terrestrial rocks. A record of metamorphic events at ~3.75, ~3.6 and ~1.7 Ga also is preserved. These discoveries approximately double, to ~40 km^2, the area over which ~4.0 Ga gneisses are known to occur. A single older zircon core in one sample suggests that rocks as old as 4.06 Ga might yet be found in the region. As early as 4.03 Ga, terrestrial differentiation was already producing tonalitic magmas, probably by partial melting of pre-existing, less differentiated crust.

Introduction

Continental crust covers about 40% of Earth's surface and is about 0.4% of Earth's volume. Archean (2.5–4.0 Ga) continental crust accounts for less than 0.05% of the planet's mass and less than 15% of the present continental area. Continental crust older than 3.8 Ga is known from only a few localities, and has a total exposure area of a few hundred square kilometres. From a planetary perspective it seems likely that Earth's first or primary crust was basaltic in composition (Taylor 1992), however most fragments of Archean crust preserved today are neither primary nor basaltic. Thus, the processes operative during the first 600 million years of Earth history must be inferred from much younger rocks.

A major issue in the study of Earth's evolution is whether the present volume of continental crust is principally the result of gradual crustal accumulation, with only limited amounts of recycling (McCulloch and Bennett 1994), or instead a 'snapshot' of an approximately steady-state condition in which formation of new crust is balanced by return of older crust to the mantle (Armstrong 1991; Bowring and Housh 1995). Stated in another way: does the relatively small amount of silicic crust older than 3.8 Ga reflect the amount of crust that formed, or is it all that remains following plate-tectonic recycling and disruption by bolide impacts? The answer to this question has far-reaching implications for a variety of issues that range from explaining the present geochemical organization of the planet, to determining the composition of Archean sea water and the role of continental crust in the emergence of life.

Identification and characterization of the few surviving fragments of ancient crust provides the most direct evidence available of the processes which shaped the early Earth. Continental crustal rocks older than 3.8 Ga are now known or inferred from the Wyoming and Slave Provinces of North America (Bowring et al. 1989; Mueller et al. 1992), northern Labrador (Collerson et al. 1991; Bridgewater and Schiotte 1991), Greenland (Nutman et al. 1996), China (Song et al. 1996), and Antarctica (Black et al. 1986). In addition, 4.1–4.3 Ga detrital zircons interpreted to have been derived from continental crust have been found in Western Australia (Froude et al. 1983, Compston and Pidgeon 1986). These discoveries show that continental crust older than 3.8 Ga was once far more voluminous and widespread than at present, and that some crustal remnants *did*

S.A. Bowring
Department of Earth Atmospheric and Planetary Sciences
Massachusetts Institute of Technology
Cambridge, MA 02139, U.S.A.
email: sbowring@mit.edu

I.S. Williams
Research School of Earth Sciences
The Australian National University
Canberra, ACT 0200
e-mail: Ian.Williams@anu.edu.au

Editorial responsibility: T.L. Grove

survive the intense meteorite bombardment early in Earth history. Furthermore, because Earth's history has been dominated by plate tectonics, the dimensions of today's Archean cratons are unlikely to reflect their original size.

The oldest rocks currently known are the Acasta gneisses (hereafter the Acasta Gneiss Complex) from the Northwest Territories of Canada (Bowring et al. 1989, 1990). In this paper we present new zircon U-Pb isotopic analyses for three samples of tonalitic to granodioritic Acasta gneiss which are significantly older than any previously described, and which together double the known areal extent of ~4.0 Ga rocks. They are the first Priscoan (>4.0 Ga: Harland et al. 1990) terrestrial rocks identified. Stern et al. (1997) have reported dates as old as 4.02 Ga from the same outcrop reported on by Bowring et al. (1989).

The Acasta Gneiss Complex

The Acasta Gneiss Complex (AGC) is exposed along the western margin of the Slave craton (Fig. 1) in the northwest corner of the Canadian Shield (Bowring et al. 1989, 1990). It consists of a heterogeneous assemblage of 3.6 to >4.0 Ga foliated to gneissic tonalites, granodiorites and granites, as well as an assortment of amphibolites and ultramafic rocks of as yet unknown age. Detailed mapping, coupled with U-Pb geochronology, has documented a complex history of intrusion and deformation.

Deformation of the complex is highly variable. In areas of high strain, finely banded gneisses consisting of layers of different age and composition are juxtaposed. In local low strain zones, however, the layering is defined by sharp contacts between rock types, and cross-cutting relationships (variably deformed) between primary igneous precursors are preserved. Samples from such low strain domains provide direct evidence for the igneous processes responsible for development of Earth's oldest known crust.

Samples for the present study were collected from a sequence of broadly layered amphibolitic and tonalitic gneisses preserved in low strain areas where the layering commonly reflects primary intrusive relationships. They are from a zone of ~4.0 Ga gneisses, which mapping has shown to extend at least 10 km south of the original discovery outcrops described by Bowring et al. (1989). Sample SAB91-63 is a gray, weakly foliated tonalitic gneiss, SAB91-37 is a foliated tonalitic gneiss from a zone of amphibolitic and tonalitic gneisses interbanded on a 10 to 45 cm scale, and SAB94-134 is a foliated, gray, granodioritic gneiss containing small (5 × 20 mm) granitic pods or segregations and cut by a dike of 3.6 Ga non-deformed granite.

Zircon U-Pb geochronology

Most zircon grains from the Acasta gneisses, having been affected by radiation damage, recrystallization and multiple thermal events, are structurally extremely complex. This is not unusual for zircon from polymetamorphic Archean terranes (e.g. Black et al. 1986; Pidgeon 1992). Isotope dilution analyses of selected Acasta zircon fragments have yielded $^{207}Pb/^{206}Pb$ ages as old as 3.98 Ga (Davidek et al. 1997), but the SHRIMP (Sensitive High Resolution Ion MicroProbe) ion-microprobe, with its high spatial resolution, is a much better means of unraveling the record of the gneisses' multi-stage thermal history preserved in the micron-scale zonation of individual zircon grains. Zircon was analyzed using both the SHRIMP I and II ion microprobes at the Australian National University. The analytical procedure broadly followed that of Williams and Claesson (1987) and Williams et al. (1996). Reference zircons SL13 (572 Ma) and AS3 (1099 Ma) were used as standards for the measurement of $^{206}Pb/^{238}U$.

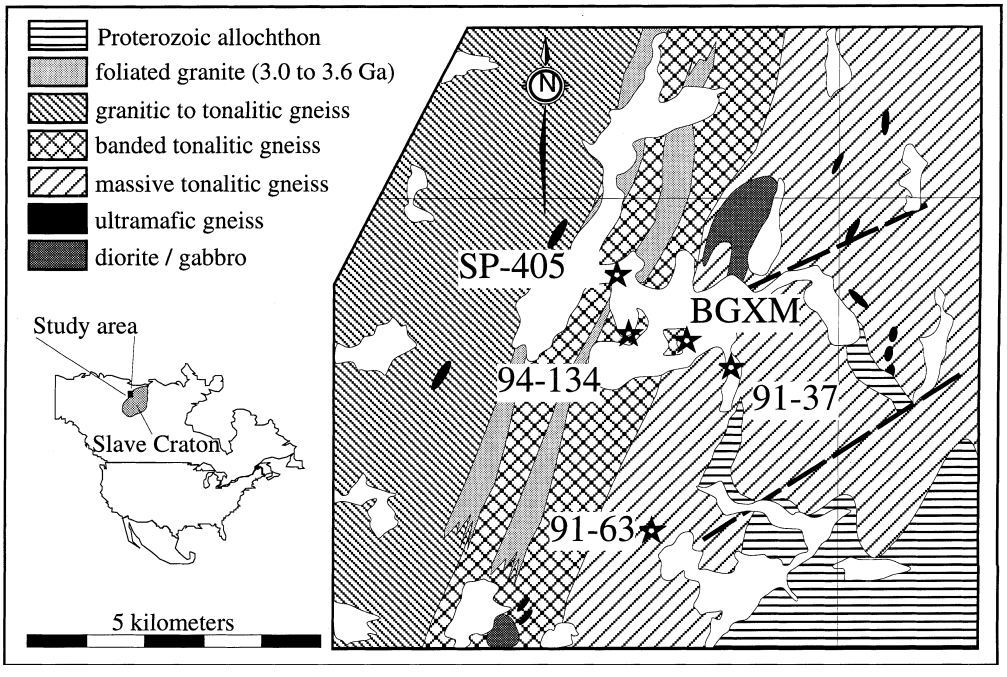

Fig. 1 Simplified geologic map of the type locality of the Acasta gneisses (Pattern free areas are lakes)

Common Pb was mostly low (< 10 ppb ^{204}Pb), and assumed to be laboratory-derived. Rare much higher common Pb contents were assumed to be due to recent redistribution of rock Pb. Ages were calculated using the constants recommended by the IUGS Subcommission on Geochronology (Steiger and Jager 1977).

Because of the zircons' complexity, particular care was required in selecting which parts of the grains were to be analyzed, and in interpreting the resulting data. Much of the zircons' internal structure could be documented in advance of analysis by optical microscopy; variable lattice damage in such ancient zircons, resulting from the competing effects of internal U and Th decay (metamictization), alteration, recrystallization, self annealing and neoblastic growth, produced marked differences in reflectance which made crystal growth structures clearly visible on the polished cross sections of the mounted grains. Once analytical work had been completed, the visibility of these structures was further enhanced by etching the sectioned surface for a few seconds with HF vapor; etching before analysis would have risked locally altering the zircons' Pb/U and Th/U.

To obtain a first-order understanding of the geochronology of the Acasta gneisses it has so far proved necessary to distinguish only a relatively small number of zircon types, while remaining aware that the appearance of such zircon can differ greatly as a function of its composition and thermal history. These types are: (1) cores – generally small zircon fragments on which later zircon has nucleated, (2) euhedrally-zoned zircon – zircon presumed to have crystallized from a fluid (probably melt) phase, (3) overgrowths – commonly unconformable to earlier structures and therefore presumed to follow a period of partial resorption, and (4) recrystallized zircon – zircon structurally and chemically modified by in situ recrystallization. Correct identification of these domains within individual crystals has proved crucial to determining which generations of zircon growth are likely to record protolith, magmatic and metamorphic ages respectively. Only in this way could the primary igneous ages of the Acasta gneisses be accurately established.

Tonalitic gneiss SAB91-63

The zircon grains from SAB91-63 are mostly turbid, inclusion rich, closely fractured, relatively equant and anhedral. A few grains (<5%) are stubby prisms with some surviving crystal faces. Damage to the original crystal structure is widespread and severe. Polished sectioning shows most grains (>80%) to consist of predominantly turbid, inclusion-rich zircon, with some zones and patches of higher clarity. Post-analysis HF etching accentuated the difference between these zircon types. Strong etching of the turbid zircon produced a mottled, mosaic texture of mostly small (<10 μm) deeply etched domains within an apparently amorphous matrix (Fig. 2A, B). Areas of clearer zircon etched more weakly, most showing no internal structure, but some disclosing remnants of simple euhedral growth zoning. The etching also revealed that most grains have thin (<10 μm), structureless partial overgrowths. In rare cases the overgrowths are thicker (up to 30 μm) and weakly zoned, or merge with small (< 50 μm) subhedral outgrowths from crystal faces.

A summary of U-Pb analyses of 19 areas within 15 grains is listed in Table 1. The analyses are highly selective in that the areas targeted were mostly those relatively rare patches of clear zircon in which either weak, simple euhedral growth zoning, or no growth zoning, was visible. For comparison, two areas with strong euhedral zoning and three areas of mottled zircon also were analyzed. Younger components in the zircon population were sampled by two analyses of overgrowths and one analysis of a prominent outgrowth. U and Th contents correlate with zircon type, being generally lower in the structureless zircon than in the zoned zircon, and being a factor of two or more higher than the former in the mottled zircon. The overgrowths and outgrowth have intermediate U contents, but relatively low Th/U.

Analyses are plotted on a concordia diagram in Fig. 3A. We prefer the diagram devised by Tera and Wasserburg (1974) rather than the traditional concordia plot of Wetherill (1956), particularly for illustrating ion-probe data, for two reasons: (1) the isotope ratios plotted are those actually measured (^{207}Pb/^{206}Pb and ^{238}U/^{206}Pb), not derivative (^{207}Pb/^{235}U), and (2) the error correlation between those ratios is very small, thereby simplifying representation and linear regression.

Considering the great antiquity of the sample, the pattern of analyses is remarkably simple; with the exception of the overgrowth data, all but two analyses form a single array which intersects concordia at about 4.0 Ga. In detail, however, the array is composite, consisting of a short horizontal branch (analyses of zircon that was isotopically disturbed only recently, possibly during the gneiss's exhumation (cf. Goldich and Mudrey 1972)) and a longer transverse branch (analyses of zircon that was isotopically disturbed in the distant past). Such branched arrays are a common feature of the SHRIMP zircon analyses from the Acasta gneisses, but only for those analyses of zircon in which the U-Pb isotopic system has been relatively well preserved. More altered zircon has isotopic compositions that are a function of the various responses of the mineral to multiple high and low temperature events, producing a scatter of data from which the age of any one of those events cannot be precisely determined.

The branched data distribution permits the age of any one zircon growth generation to be calculated by two partly independent methods. First the age can be calculated from the horizontal branch, using those analyses with highest equal radiogenic ^{207}Pb/^{206}Pb. Secondly, the age can be calculated by assuming that the ancient isotopic disturbance was caused mainly by one

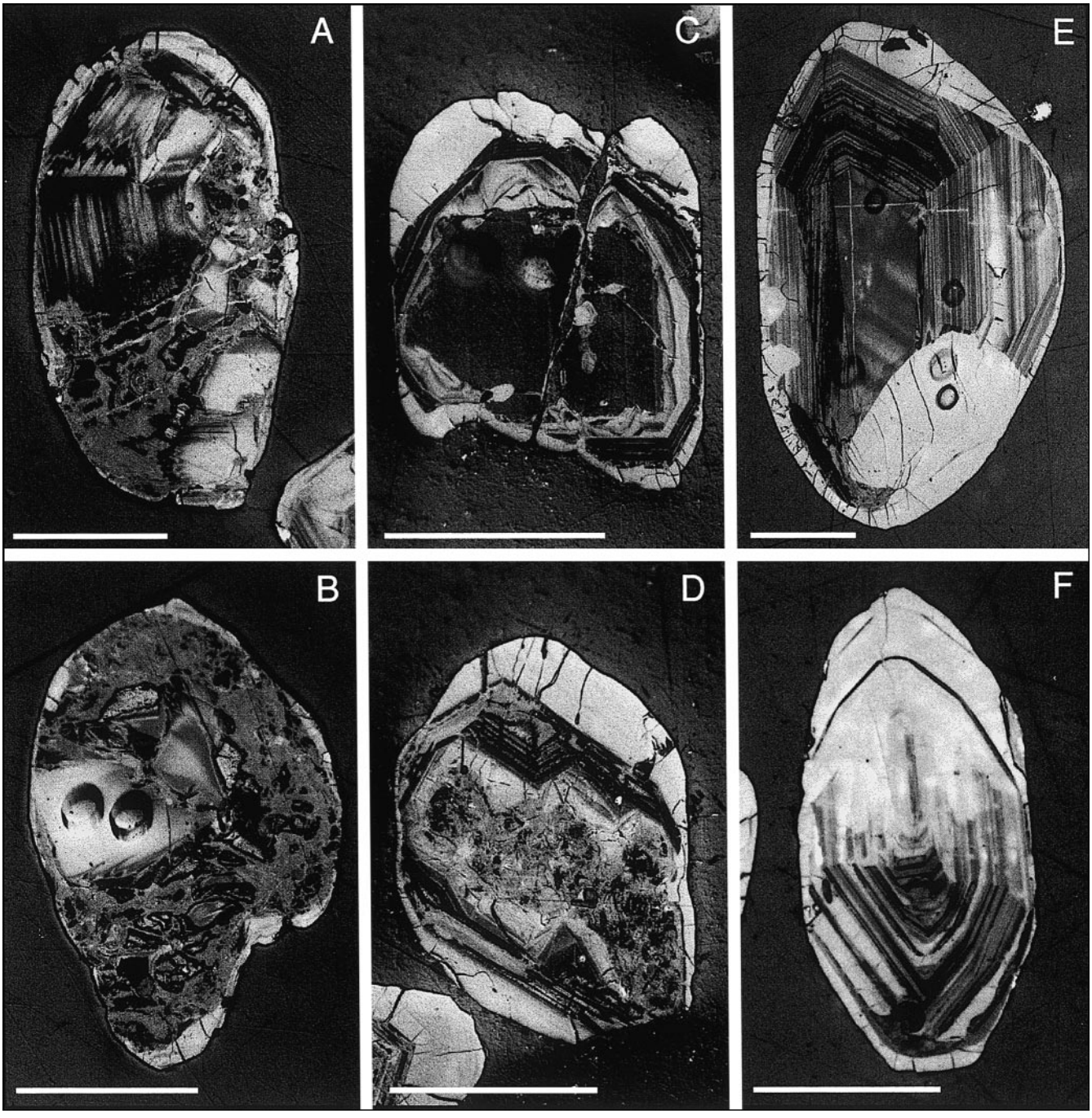

event and regressing the transverse array. In the ideal case, the two ages obtained using different subsets of the data will be the same within analytical uncertainty.

The nine highest radiogenic $^{207}Pb/^{206}Pb$ measurements of the 14 comprising the main group are equal within analytical uncertainty (MSWD = 1.1). These are all the analyses of structureless or zoned zircon, except for analyses 1.1 and 9.1. The weighted mean value of 0.4254 ± 0.0004 (σ) is equivalent to an age of 4002 ± 4 Ma (tσ), where t is Student's t multiplier and tσ therefore the 95% confidence limit. The two omitted analyses, plus the three analyses of mottled zircon, lie on a linear array which also includes analyses 2.1 and 14.1 (MSWD = 1.95). The concordia intersections of that line are 3993 ± 5 Ma (tσ) and 1225 $^{+185}_{-205}$ Ma (tσ). The upper intersection is indistinguishable from the mean $^{207}Pb/^{206}Pb$ age, supporting the argument that the branched array reflects isotopic disturbance of a single zircon generation at two different times. The higher U, now more altered zircon, has responded to the earlier event – the lower U, less altered zircon, apparently has not. Because the horizontal array is defined by analyses of the least altered zircon and probably reflects only recent Pb loss, we consider it to give the most accurate estimate of the zircon crystallization age, 4002 ± 4 Ma.

◀

Fig. 2A–F Reflected light photomicrographs of sectioned, polished, HF-etched zircon grains. Scale bars 100 μm. **A** SAB91-63 Crystal showing areas with well or partly preserved simple euhedral growth zoning separated by a region where the crystal structure has been destroyed by alteration, in part associated with fractures. The grain is mostly surrounded by a thin overgrowth. **B** SAB91-63 Grain 15. A small area of old (≥4.06 Ga) structureless zircon preserved within a grain consisting mainly of a mottled mosaic of variously altered zircon within a complexly structured, relatively amorphous matrix. The grain is surrounded by a thin overgrowth. **C** SAB91-37 Grain 17. A fragment of simply growth zoned zircon enclosed within a complex, composite overgrowth consisting of an early growth of zoned, multifaceted zircon, overgrown and infilled by more strongly zoned zircon of much simpler crystal form, discordantly overgrown in turn by a thick, structureless layer. The zoned center is ~4.0 Ga, the intermediate layers and overgrowth ~3.6 Ga. **D** SAB91-37 Grain consisting mainly of composite overgrowth, showing a well-developed multifaceted inner layer, infilled and overgrown by more strongly zoned zircon, surrounded in turn by a thick, structureless overgrowth. The center of the grain is now a chaotic mosaic of altered zircon in a relatively amorphous matrix. **E** SAB94-134 Grain 1. A very large grain consisting mainly of well preserved, simply zoned zircon, five analyses of which (note sputter pits) yield ≥4.0 Ga. A similar age is obtained from the two analyses in the large, sharply-defined region of recrystallization at the lower right side. The grain is surrounded by a rarely-developed thin overgrowth that could be distinguished from recrystallized zircon by its zoning pattern and brighter cathodoluminescence. **F** SAB94-134 Grain 26. Partly recrystallized grain. Original euhedral growth zoning, still preserved at the lower end, has been almost completely destroyed at the upper end, but is still visible as weak ghost zoning near the center. The analysis near center gave a concordant isotopic composition midway between that of zoned and wholly recrystallized zircon in other grains

The two analyses with higher $^{207}Pb/^{206}Pb$ than the main array (15.1, 15.2) are both from one small (100 μm diameter) area of clear, unzoned zircon within an otherwise mottled grain (Fig 2B). An analysis of the mottled area (15.3) falls within the main array. The clear area is probably the remains of a core, although no growth structure survives in the surrounding mottled zircon that proves this. The two analyses are nearly concordant, giving a minimum age for the core of 4065 ± 8 Ma (σ). The three analyses of overgrowths, in contrast, are discordant and not collinear. Two of those analyses give the same $^{207}Pb/^{206}Pb$ age however (3.73 Ga), which is a minimum estimate of the overgrowths' crystallization age.

The 4002 Ma zircon has U and Th contents common in zircon from tonalites and, more importantly, in many places preserves remnants of the simple, fine, prismatic euhedral growth zoning that is a feature of zircon precipitated from granitoid magmas (Fig 2A). That zoning is sharply truncated against the overgrowths, which are unzoned or weakly zoned and significantly lower in Th/U, both common features of metamorphic zircon. The pattern of truncated zoning shows that prior to metamorphism the zircons were very much larger, indicating physical or chemical breakdown of the grains before, or in the early stages of, the metamorphic event.

Together, the zircon analyses and crystal structures indicate at least three phases of zircon growth, one at ≥4065 Ma, found only in a single core, one at 4002 Ma, which produced the great bulk of the zircon population, and one at ~3730 Ma, which produced thin overgrowths and outgrowths. The most straightforward interpretation is that an igneous rock 4002 Ma old, containing inheritance ≥4065 Ma old, was metamorphosed ~3730 Ma ago, and the zircon chemical compositions and microstructures strongly support this.

Tonalitic gneiss SAB91-37

The zircons from SAB91-37 are mostly large (100–200 μm diameter), subhedral to anhedral grains with few preserved crystal faces. The mean aspect ratio is about 2, the smaller grains generally being the more prismatic. Most grains, in particular the larger ones, consist of a turbid center surrounded by a relatively clear mantle. The turbidity is due to high concentrations of fine inclusions and fractures, as well as cloudiness of the zircon itself.

Light HF etching of the sectioned grains after analysis revealed many structures that had not been visible beforehand (Fig 2C, D). There are three main generations of crystal growth; centers, overgrowths, and an intermediate layer between. Most centers are extremely complex, consisting of a mottled mosaic of inclusions and remnants of structureless or euhedrally zoned zircon within an apparently amorphous matrix. The intermediate layer is composite and, in most grains, not well developed or preserved. Where well developed near crystal terminations, this layer consists of an inner layer of multiple pyramids of euhedrally zoned zircon grown on high points on the former surface of the zircon, later infilled and overgrown by an outer layer of strongly zoned zircon with a much simpler crystal form. Along prism faces, the inner layer is thinner and composed of zircon with undulose zonation. Clear, structureless or weakly zoned mantles have in turn overgrown the intermediate layer either conformably or with minor unconformity. The mantles commonly are preserved only near the terminations of grains, where in some rare cases they reach a thickness of over 100 μm.

Analyses of SAB91-37 zircon are listed in Table 1, subdivided according to the type of zircon sampled. Analyses of the centers are further subdivided according to the pattern and strength of zoning; those regions where zoning appears to have been lost due to recrystallization are identified separately. A feature of the data is the systematic differences in U and Th content between zircon types (Fig 4). For example, the highest Th contents and Th/U values are found in the centers, where average Th/U decreases with increasing strength of zonation. Th is consistently low (<165 ppm) in the overgrowths, recrystallized areas and intermediate layers, in particular the last have very low Th/U (0.05–0.13).

The distribution of U-Pb isotopic compositions is illustrated in Fig. 3B. Two clusters of analyses dominate the diagram, one close to 4.0 Ga and the other close to

Table 1 Summary of Acasta zircon U-Th-Pb isotopic compositions (uncertainties one standard error)

Grain	Zircon type	Pb[a] (ppm)	U (ppm)	Th (ppm)	$\frac{Th}{U}$	Common[b] ^{206}Pb(%)	Apparent age (Ma)						
							$\frac{^{207}Pb^a}{^{206}Pb}$	$\frac{^{208}Pb^a}{^{206}Pb}$	$\frac{^{208}Pb^a}{^{232}Th}$	$\frac{^{206}Pb^a}{^{232}U}$	$\frac{^{208}Pb}{^{232}Th}$	$\frac{^{206}Pb}{^{232}U}$	$\frac{^{207}Pb}{^{206}Pb}$
Tonalitic gneiss SAB91-63													
6.1	Structureless	248	217	117	0.54	0.011	0.4279 ± 24	0.1419 ± 11	0.2220 ± 31	0.8448 ± 84	4052 ± 51	3948 ± 29	4010 ± 8
12.1	Structureless	331	304	150	0.49	0.016	0.4291 ± 22	0.1269 ± 15	0.2091 ± 32	0.8125 ± 69	3837 ± 53	3834 ± 25	4014 ± 8
15.1	Structureless	347	304	84	0.28	0.006	0.4439 ± 22	0.0702 ± 10	0.2227 ± 40	0.8759 ± 86	4064 ± 67	4055 ± 29	4065 ± 8
15.2	Structureless	554	478	163	0.34	0.011	0.4364 ± 19	0.0873 ± 5	0.2265 ± 23	0.8845 ± 63	4127 ± 37	4085 ± 21	4039 ± 7
8.2	Weakly zoned	234	201	114	0.57	0.027	0.4271 ± 16	0.1449 ± 9	0.2188 ± 28	0.8577 ± 85	3999 ± 47	3992 ± 30	4007 ± 6
1.1	Weakly zoned	349	305	194	0.64	0.016	0.4205 ± 10	0.1652 ± 15	0.2171 ± 28	0.8368 ± 65	3970 ± 46	3920 ± 23	3984 ± 4
14.1	Weakly zoned	399	341	246	0.72	0.016	0.4237 ± 11	0.1860 ± 12	0.2177 ± 28	0.8432 ± 81	3981 ± 46	3942 ± 28	3995 ± 4
4.1	Weakly zoned	391	347	229	0.66	0.005	0.4256 ± 8	0.1711 ± 7	0.2127 ± 20	0.8188 ± 60	3898 ± 34	3856 ± 21	4002 ± 3
3.1	Weakly zoned	447	388	279	0.72	0.016	0.4251 ± 12	0.1859 ± 18	0.2145 ± 37	0.8291 ± 103	3928 ± 62	3892 ± 36	4000 ± 4
11.1	Weakly zoned	657	556	428	0.77	0.016	0.4267 ± 15	0.1951 ± 18	0.2144 ± 28	0.8460 ± 68	3926 ± 46	3952 ± 24	4006 ± 5
2.1	Weakly zoned	653	558	432	0.77	0.016	0.4238 ± 16	0.1977 ± 16	0.2141 ± 29	0.8383 ± 82	3922 ± 48	3925 ± 29	3996 ± 6
9.1	Strongly zoned	425	414	268	0.65	0.011	0.4086 ± 17	0.1751 ± 8	0.2039 ± 27	0.7523 ± 81	3750 ± 45	3616 ± 30	3941 ± 6
10.1	Strongly zoned	615	541	458	0.85	0.016	0.4251 ± 11	0.2032 ± 15	0.1944 ± 23	0.8098 ± 67	3590 ± 39	3824 ± 24	4000 ± 4
7.1	Mottled	1092	900	819	0.91	0.006	0.4208 ± 5	0.2324 ± 6	0.2175 ± 17	0.8517 ± 55	3978 ± 28	3972 ± 19	3985 ± 2
15.3	Mottled	940	990	366	0.37	0.032	0.4046 ± 10	0.0984 ± 3	0.1952 ± 18	0.7335 ± 54	3603 ± 30	3547 ± 20	3926 ± 4
13.1	Mottled	1218	1051	1024	0.97	0.027	0.4145 ± 13	0.2524 ± 9	0.2092 ± 18	0.8068 ± 57	3839 ± 30	3814 ± 20	3962 ± 5
5.1	Overgrowth	440	515	142	0.28	0.019	0.3555 ± 11	0.0722 ± 3	0.1821 ± 16	0.6953 ± 44	3382 ± 27	3403 ± 17	3731 ± 5
4.2	Overgrowth	452	586	101	0.17	0.005	0.3149 ± 16	0.0458 ± 4	0.1750 ± 23	0.6593 ± 50	3260 ± 40	3264 ± 20	3545 ± 8
8.1	Outgrowth	538	634	42	0.07	0.002	0.3557 ± 12	0.0173 ± 2	0.1879 ± 23	0.7184 ± 43	3481 ± 39	3490 ± 16	3731 ± 5
Tonalitic gneiss SAB91-37													
28.1	Structureless	181	169	112	0.66	0.080	0.4090 ± 34	0.1838 ± 22	0.2165 ± 59	0.7818 ± 165	3961 ± 98	3723 ± 60	3943 ± 13
49.1	Structureless	305	270	270	1.00	0.200	0.4205 ± 30	0.2703 ± 18	0.2096 ± 48	0.7750 ± 134	3847 ± 80	3699 ± 49	3984 ± 11
37.1	Structureless	361	320	235	0.73	0.003	0.4249 ± 18	0.1981 ± 18	0.2177 ± 55	0.8073 ± 172	3981 ± 92	3815 ± 61	4000 ± 6
42.1	Structureless	376	343	83	0.24	0.016	0.4302 ± 12	0.0619 ± 6	0.2181 ± 49	0.8531 ± 149	3988 ± 81	3977 ± 52	4018 ± 4
36.1	Structureless	395	368	260	0.71	0.304	0.4213 ± 44	0.2238 ± 27	0.2403 ± 53	0.7585 ± 126	4353 ± 86	3639 ± 46	3987 ± 16
26.1	Structureless	850	799	551	0.69	0.049	0.4038 ± 17	0.1839 ± 17	0.2073 ± 47	0.7779 ± 139	3807 ± 80	3710 ± 51	3923 ± 6
13.2	Weakly zoned	260	251	151	0.60	0.407	0.4147 ± 34	0.1620 ± 28	0.2050 ± 58	0.7626 ± 146	3769 ± 98	3654 ± 53	3963 ± 12
24.5	Weakly zoned	290	256	187	0.73	0.243	0.4268 ± 117	0.2178 ± 80	0.2387 ± 138	0.8012 ± 324	4327 ± 226	3793 ± 117	4006 ± 42
24.3	Weakly zoned	347	302	241	0.80	0.020	0.4350 ± 37	0.2020 ± 16	0.2063 ± 46	0.8134 ± 151	3971 ± 78	3837 ± 54	4035 ± 13
13.1	Weakly zoned	382	322	249	0.77	0.084	0.4302 ± 26	0.2006 ± 19	0.2186 ± 54	0.8438 ± 173	3996 ± 90	3944 ± 61	4018 ± 9
32.1	Weakly zoned	413	355	295	0.83	0.032	0.4170 ± 10	0.2180 ± 12	0.2167 ± 41	0.8260 ± 134	3964 ± 69	3882 ± 48	3972 ± 4
13.4	Weakly zoned	470	402	321	0.80	0.017	0.4284 ± 28	0.2048 ± 22	0.2131 ± 58	0.8315 ± 183	3905 ± 97	3901 ± 65	4012 ± 10
39.1	Weakly zoned	508	451	317	0.70	0.024	0.4159 ± 16	0.1824 ± 17	0.2126 ± 43	0.8191 ± 117	3896 ± 72	3857 ± 42	3968 ± 6
17.1	Weakly zoned	657	557	579	1.04	0.025	0.4237 ± 24	0.2583 ± 25	0.2025 ± 43	0.8140 ± 139	3727 ± 73	3839 ± 50	3995 ± 9
39.2	Weakly zoned	589	562	261	0.47	0.047	0.4261 ± 26	0.1216 ± 15	0.2058 ± 43	0.7867 ± 121	3782 ± 71	3741 ± 44	4004 ± 9
17.2	Weakly zoned	824	688	822	1.20	0.043	0.4206 ± 12	0.3048 ± 18	0.2055 ± 38	0.8058 ± 128	3778 ± 64	3810 ± 46	3984 ± 4
8.1	Strongly zoned	355	369	150	0.41	0.032	0.3644 ± 26	0.1088 ± 25	0.2024 ± 83	0.7591 ± 218	3725 ± 139	3641 ± 80	3768 ± 11
6.1	Strongly zoned	352	371	288	0.78	0.465	0.3595 ± 25	0.2375 ± 33	0.2106 ± 65	0.6890 ± 158	3864 ± 108	3379 ± 61	3748 ± 10
43.1	Strongly zoned	356	381	285	0.75	0.122	0.3225 ± 38	0.2121 ± 44	0.2005 ± 63	0.7074 ± 161	3693 ± 107	3449 ± 61	3582 ± 18
48.1	Strongly zoned	447	422	307	0.73	0.377	0.4018 ± 46	0.2134 ± 38	0.2236 ± 74	0.7626 ± 184	4079 ± 123	3654 ± 68	3916 ± 17
13.6	Strongly zoned	599	500	466	0.93	0.076	0.4304 ± 26	0.2396 ± 22	0.2139 ± 42	0.8323 ± 124	3919 ± 70	3904 ± 44	4019 ± 9
8.2	Strongly zoned	516	531	230	0.43	0.036	0.3607 ± 14	0.1131 ± 11	0.2003 ± 50	0.7665 ± 146	3690 ± 85	3668 ± 53	3753 ± 6
27.1	Strongly zoned	527	535	188	0.35	0.118	0.4026 ± 24	0.0923 ± 12	0.2014 ± 57	0.7667 ± 167	3709 ± 96	3669 ± 61	3919 ± 9
18.1	Strongly zoned	638	557	443	0.79	0.070	0.4236 ± 19	0.2094 ± 12	0.2146 ± 44	0.8142 ± 142	3930 ± 73	3840 ± 51	3995 ± 7
27.2	Strongly zoned	511	585	119	0.20	0.081	0.3517 ± 15	0.0562 ± 9	0.1994 ± 46	0.7215 ± 108	3676 ± 78	3502 ± 41	3714 ± 7
41.1	Strongly zoned	698	637	576	0.90	0.023	0.4221 ± 8	0.2297 ± 11	0.1957 ± 34	0.7699 ± 113	3613 ± 57	3680 ± 41	3990 ± 3

34.1	Strongly zoned	800	723	350	0.48	0.013	0.4297 ± 28	0.1264 ± 21	0.2159 ± 51	0.8265 ± 133	3951 ± 85	3883 ± 47	4016 ± 10
46.3	Strongly zoned	842	738	619	0.84	0.016	0.4252 ± 40	0.2285 ± 25	0.2181 ± 62	0.8002 ± 167	3987 ± 104	3790 ± 60	4001 ± 14
8.4	Strongly zoned	735	745	429	0.58	0.017	0.3613 ± 20	0.1496 ± 13	0.1971 ± 38	0.7578 ± 114	3636 ± 65	3636 ± 42	3755 ± 8
13.5	Strongly zoned	899	757	722	0.95	0.013	0.4223 ± 19	0.2434 ± 19	0.2111 ± 56	0.8269 ± 172	3871 ± 94	3885 ± 61	3991 ± 7
24.1	Strongly zoned	935	799	930	1.16	0.019	0.4223 ± 17	0.2991 ± 21	0.2026 ± 58	0.7890 ± 197	3729 ± 98	3749 ± 71	3991 ± 6
24.4	Strongly zoned	888	818	1013	1.24	0.182	0.4145 ± 30	0.3266 ± 19	0.1907 ± 50	0.7237 ± 152	3528 ± 85	3510 ± 57	3962 ± 11
25.1	Strongly zoned	784	854	672	0.79	0.012	0.3216 ± 17	0.2092 ± 16	0.1852 ± 43	0.6963 ± 138	3434 ± 74	3406 ± 53	3578 ± 8
18.2	Strongly zoned	1113	909	1167	1.28	0.034	0.4204 ± 41	0.3242 ± 37	0.2057 ± 63	0.8139 ± 199	3781 ± 107	3839 ± 71	3984 ± 15
23.1	Mottled	477	438	332	0.76	0.070	0.4094 ± 89	0.2037 ± 87	0.2105 ± 161	0.7842 ± 374	3862 ± 271	3732 ± 137	3944 ± 33
16.1	Mottled	413	466	98	0.21	0.047	0.3584 ± 36	0.0670 ± 12	0.2308 ± 86	0.7217 ± 208	4197 ± 142	3503 ± 78	3743 ± 15
29.1	Mottled	761	673	516	0.77	0.051	0.4119 ± 30	0.1962 ± 24	0.2088 ± 63	0.8159 ± 176	3834 ± 106	3846 ± 63	3953 ± 11
23.3	Mottled	631	741	164	0.22	0.071	0.3340 ± 30	0.0685 ± 17	0.2185 ± 97	0.7053 ± 159	3994 ± 161	3441 ± 61	3635 ± 14
29.2	Mottled	763	833	368	0.44	0.053	0.3782 ± 35	0.1199 ± 15	0.1928 ± 54	0.7102 ± 153	3564 ± 91	3459 ± 58	3825 ± 14
37.2	Mottled	735	926	328	0.35	0.410	0.3448 ± 15	0.1752 ± 206	0.2995 ± 362	0.6060 ± 116	5295 ± 570	3054 ± 47	3684 ± 7
23.2	Mottled	1075	938	865	0.92	0.035	0.4220 ± 17	0.2378 ± 16	0.2067 ± 69	0.8014 ± 231	3797 ± 115	3794 ± 83	3989 ± 6
46.1	Mottled	1230	1036	933	0.90	0.005	0.4251 ± 7	0.2368 ± 7	0.2180 ± 43	0.8294 ± 142	3986 ± 71	3893 ± 50	4000 ± 3
20.2	Mottled	998	1134	531	0.47	0.031	0.3737 ± 11	0.1305 ± 8	0.1892 ± 43	0.6792 ± 100	3502 ± 72	3341 ± 38	3807 ± 4
45.1	Mottled	1065	1961	1553	0.79	0.055	0.2736 ± 33	0.2500 ± 39	0.1307 ± 30	0.4141 ± 68	2483 ± 54	2233 ± 31	3327 ± 19
38.2	Intermediate layer	453	570	67	0.12	0.018	0.3231 ± 20	0.0329 ± 8	0.1901 ± 62	0.6816 ± 133	3518 ± 106	3350 ± 51	3585 ± 10
47.1	Intermediate layer	474	609	46	0.08	0.033	0.3127 ± 20	0.0225 ± 5	0.2036 ± 62	0.6775 ± 108	3746 ± 104	3335 ± 42	3534 ± 10
15.1	Intermediate layer	433	633	80	0.13	0.005	0.2957 ± 11	0.0379 ± 7	0.1796 ± 68	0.5960 ± 162	3339 ± 118	3014 ± 66	3448 ± 6
35.1	Intermediate layer	492	650	37	0.06	0.012	0.3040 ± 9	0.0151 ± 9	0.1775 ± 114	0.6680 ± 108	3303 ± 197	3298 ± 42	3491 ± 5
50.1	Intermediate layer	511	673	88	0.13	0.030	0.3071 ± 54	0.0407 ± 21	0.2026 ± 126	0.6544 ± 211	3729 ± 213	3245 ± 83	3507 ± 27
24.2	Intermediate layer	635	820	60	0.07	0.043	0.3113 ± 16	0.0204 ± 6	0.1884 ± 81	0.6763 ± 179	3488 ± 138	3330 ± 69	3527 ± 8
2.1	Intermediate layer	684	900	67	0.07	0.025	0.3134 ± 22	0.0175 ± 8	0.1562 ± 73	0.6637 ± 105	2933 ± 128	3281 ± 41	3538 ± 11
31.1	Intermediate layer	884	1130	48	0.04	0.004	0.3162 ± 10	0.0110 ± 3	0.1789 ± 50	0.6851 ± 84	3326 ± 85	3364 ± 32	3551 ± 5
22.1	Intermediate layer	888	1221	88	0.07	0.086	0.3050 ± 23	0.0227 ± 7	0.2011 ± 77	0.6364 ± 119	3703 ± 129	3175 ± 47	3496 ± 12
11.1	Intermediate layer	750	1385	92	0.07	0.055	0.2495 ± 6	0.0219 ± 4	0.1636 ± 46	0.4953 ± 82	3062 ± 80	2594 ± 36	3182 ± 4
19.1	Intermediate layer	759	1660	85	0.05	0.078	0.2196 ± 14	0.0149 ± 7	0.1252 ± 58	0.4306 ± 57	2384 ± 104	2309 ± 26	2978 ± 10
44.1	Intermediate layer	892	1737	163	0.09	0.013	0.2420 ± 16	0.0266 ± 4	0.1331 ± 36	0.4703 ± 92	2526 ± 65	2485 ± 40	3133 ± 10
21.3	Intermediate layer	1346	2429	119	0.05	0.026	0.2556 ± 11	0.0150 ± 3	0.1549 ± 39	0.5072 ± 68	2910 ± 68	2645 ± 29	3220 ± 7
13.3	Overgrowth	78	84	59	0.71	0.016	0.3174 ± 72	0.1805 ± 68	0.1846 ± 116	0.7225 ± 337	3424 ± 200	3506 ± 127	3557 ± 35
1.1	Overgrowth	105	115	83	0.73	0.024	0.3248 ± 50	0.1980 ± 60	0.1899 ± 111	0.6968 ± 310	3514 ± 190	3409 ± 119	3593 ± 24
21.1	Overgrowth	150	149	154	1.03	0.171	0.3319 ± 64	0.2733 ± 61	0.1926 ± 78	0.7285 ± 219	3560 ± 133	3528 ± 82	3626 ± 30
4.1	Overgrowth	105	153	5	0.03	0.079	0.2646 ± 31	0.0079 ± 15	0.1446 ± 282	0.6256 ± 242	2731 ± 504	3132 ± 97	3275 ± 19
46.2	Overgrowth	187	245	51	0.21	0.103	0.3090 ± 52	0.0677 ± 34	0.2094 ± 127	0.6429 ± 202	3843 ± 214	3200 ± 80	3516 ± 26
33.1	Overgrowth	209	246	79	0.32	0.030	0.3099 ± 22	0.0874 ± 15	0.1915 ± 55	0.7053 ± 144	3542 ± 94	3441 ± 55	3520 ± 11
9.1	Overgrowth	230	277	112	0.41	0.103	0.3123 ± 21	0.1088 ± 34	0.1824 ± 70	0.6798 ± 135	3387 ± 120	3344 ± 52	3532 ± 11
12.1	Overgrowth	269	307	109	0.36	0.019	0.3157 ± 31	0.0935 ± 20	0.1899 ± 59	0.7207 ± 145	3514 ± 100	3499 ± 55	3549 ± 15
18.3	Overgrowth	267	315	98	0.31	0.009	0.3229 ± 35	0.0819 ± 24	0.1837 ± 70	0.7018 ± 152	3409 ± 120	3427 ± 58	3584 ± 17
10.1	Overgrowth	282	333	114	0.34	0.016	0.3108 ± 18	0.0930 ± 16	0.1896 ± 57	0.6994 ± 148	3509 ± 98	3418 ± 56	3525 ± 9
8.3	Overgrowth	297	345	112	0.33	0.119	0.3163 ± 18	0.0889 ± 18	0.1948 ± 58	0.7131 ± 133	3597 ± 98	3470 ± 50	3552 ± 9
30.1	Overgrowth	352	406	131	0.32	0.016	0.3244 ± 20	0.0859 ± 13	0.1900 ± 42	0.7158 ± 104	3516 ± 72	3480 ± 39	3591 ± 10
21.2	Overgrowth	321	421	98	0.23	0.218	0.3045 ± 40	0.0600 ± 27	0.1680 ± 89	0.6495 ± 165	3139 ± 155	3226 ± 65	3493 ± 20
20.1	Overgrowth	371	434	143	0.33	0.046	0.3177 ± 40	0.0877 ± 22	0.1875 ± 74	0.7055 ± 195	3474 ± 127	3441 ± 74	3559 ± 20
5.1	Recrystallized	95	99	59	0.60	0.277	0.3271 ± 29	0.1549 ± 41	0.1950 ± 112	0.7551 ± 329	3600 ± 190	3626 ± 122	3604 ± 13
14.1	Recrystallized	116	150	126	0.84	0.859	0.3099 ± 58	0.3060 ± 108	0.2027 ± 121	0.5583 ± 231	3731 ± 204	2859 ± 96	3521 ± 29
3.1	Recrystallized	94	151	83	0.55	0.564	0.2934 ± 36	0.2085 ± 53	0.1830 ± 72	0.4807 ± 124	3397 ± 123	2530 ± 54	3436 ± 19
40.1	Recrystallized	161	177	84	0.47	0.779	0.3237 ± 33	0.2324 ± 72	0.3335 ± 131	0.6776 ± 146	5817 ± 199	3335 ± 56	3588 ± 16
7.1	Recrystallized	215	256	126	0.49	0.510	0.3160 ± 35	0.1521 ± 38	0.2057 ± 74	0.6662 ± 154	3780 ± 124	3291 ± 60	3551 ± 17
9.2	Recrystallized	283	307	143	0.47	0.009	0.3264 ± 23	0.1254 ± 19	0.1983 ± 74	0.7369 ± 226	3657 ± 126	3559 ± 84	3600 ± 11
38.1	Recrystallized	353	441	67	0.15	0.084	0.3484 ± 29	0.0467 ± 11	0.2058 ± 73	0.6674 ± 156	3783 ± 122	3296 ± 60	3700 ± 13

Table 1 (Continued)

Grain	Zircon type	Pb^a (ppm)	U (ppm)	Th (ppm)	$\frac{Th}{U}$	Common ^{206}Pb(%)[b]	Apparent age (Ma)						
							$\frac{^{207}Pb^a}{^{206}Pb}$	$\frac{^{208}Pb^a}{^{206}Pb}$	$\frac{^{208}Pb^a}{^{232}Th}$	$\frac{^{206}Pb^a}{^{232}U}$	$\frac{^{208}Pb}{^{232}Th}$	$\frac{^{206}Pb}{^{232}U}$	$\frac{^{207}Pb}{^{206}Pb}$
Granodioritic gneiss SAB94-134													
7.3	Weakly zoned	294	263	69	0.26	0.001	0.4273 ± 22	0.0678 ± 5	0.2240 ± 34	0.8696 ± 108	4085 ± 56	4034 ± 37	4008 ± 8
7.2	Weakly zoned	341	303	93	0.31	0.003	0.4290 ± 13	0.0773 ± 6	0.2195 ± 38	0.8670 ± 123	4011 ± 63	4025 ± 43	4014 ± 4
7.1	Weakly zoned	339	321	96	0.30	0.004	0.4135 ± 16	0.0770 ± 5	0.2116 ± 31	0.8246 ± 99	3879 ± 52	3877 ± 35	3959 ± 6
7.5	Weakly zoned	366	325	94	0.29	0.015	0.4349 ± 8	0.0742 ± 4	0.2228 ± 36	0.8681 ± 117	4065 ± 60	4029 ± 40	4034 ± 3
4.2	Weakly zoned	363	340	101	0.30	0.017	0.4029 ± 13	0.0744 ± 7	0.2106 ± 34	0.8385 ± 104	3862 ± 56	3925 ± 37	3920 ± 5
3.3	Weakly zoned	373	344	103	0.30	0.158	0.4238 ± 12	0.0787 ± 7	0.2198 ± 40	0.8385 ± 126	4015 ± 67	3926 ± 44	3996 ± 4
7.4	Weakly zoned	378	350	110	0.31	0.004	0.4177 ± 12	0.0801 ± 7	0.2142 ± 40	0.8366 ± 125	3923 ± 67	3919 ± 44	3974 ± 4
1.4	Weakly zoned	473	414	136	0.33	0.012	0.4355 ± 16	0.0835 ± 13	0.2218 ± 45	0.8736 ± 108	4050 ± 75	4047 ± 37	4036 ± 6
11.1	Weakly zoned	504	449	156	0.35	0.019	0.4338 ± 7	0.0870 ± 4	0.2148 ± 30	0.8580 ± 102	3933 ± 49	3994 ± 35	4031 ± 3
11.3	Weakly zoned	494	453	144	0.32	0.006	0.4364 ± 33	0.0807 ± 10	0.2118 ± 39	0.8362 ± 111	3883 ± 66	3918 ± 39	4040 ± 11
24.1	Weakly zoned	503	456	180	0.39	0.015	0.4222 ± 33	0.1023 ± 5	0.2179 ± 33	0.8402 ± 109	3984 ± 55	3932 ± 38	3990 ± 12
3.5	Weakly zoned	535	486	164	0.34	0.135	0.4245 ± 12	0.0884 ± 5	0.2221 ± 32	0.8453 ± 105	4054 ± 53	3949 ± 37	3998 ± 4
11.6	Weakly zoned	542	490	166	0.34	0.056	0.4338 ± 8	0.0871 ± 3	0.2170 ± 28	0.8459 ± 99	3969 ± 47	3951 ± 35	4030 ± 3
1.3	Weakly zoned	578	507	185	0.36	0.002	0.4332 ± 20	0.0918 ± 5	0.2186 ± 30	0.8677 ± 104	3996 ± 50	4027 ± 36	4028 ± 7
3.1	Weakly zoned	580	508	170	0.33	0.013	0.4315 ± 16	0.0856 ± 4	0.2234 ± 30	0.8737 ± 103	4075 ± 49	4048 ± 36	4023 ± 5
1.2	Weakly zoned	552	515	189	0.37	0.001	0.4168 ± 15	0.0937 ± 7	0.2102 ± 31	0.8238 ± 99	3857 ± 52	3874 ± 35	3971 ± 6
12.1	Weakly zoned	496	528	233	0.44	0.008	0.3639 ± 22	0.1141 ± 11	0.1909 ± 33	0.7386 ± 100	3531 ± 56	3565 ± 37	3766 ± 9
22.2	Weakly zoned	444	532	83	0.16	0.002	0.3134 ± 6	0.0414 ± 3	0.1901 ± 29	0.7157 ± 85	3518 ± 49	3480 ± 32	3538 ± 3
2.2	Weakly zoned	555	537	142	0.27	0.012	0.4069 ± 10	0.0681 ± 9	0.2092 ± 38	0.8140 ± 93	3839 ± 64	3839 ± 33	3935 ± 4
3.4	Weakly zoned	588	541	156	0.29	0.024	0.4246 ± 16	0.0742 ± 7	0.2166 ± 37	0.8428 ± 114	3963 ± 62	3941 ± 40	3999 ± 6
12.2	Weakly zoned	582	545	249	0.46	0.026	0.4064 ± 9	0.1172 ± 6	0.2090 ± 27	0.8138 ± 92	3836 ± 45	3838 ± 33	3933 ± 3
8.1	Weakly zoned	559	549	125	0.23	0.002	0.4127 ± 24	0.0582 ± 3	0.2065 ± 29	0.8046 ± 98	3794 ± 48	3806 ± 35	3956 ± 9
4.1	Weakly zoned	629	557	256	0.46	0.015	0.4274 ± 6	0.1180 ± 6	0.2177 ± 30	0.8479 ± 102	3981 ± 50	3958 ± 36	4008 ± 2
11.5	Weakly zoned	600	566	203	0.36	0.256	0.4182 ± 27	0.2112 ± 8	0.2112 ± 32	0.8139 ± 97	3873 ± 54	3839 ± 35	3976 ± 10
26.1	Weakly zoned	666	616	213	0.35	0.004	0.4020 ± 17	0.0890 ± 3	0.2166 ± 27	0.8429 ± 98	3963 ± 45	3941 ± 34	3917 ± 6
10.1	Strongly zoned	615	611	235	0.39	1.003	0.3914 ± 18	0.1080 ± 14	0.2187 ± 38	0.7805 ± 90	3998 ± 64	3719 ± 33	3876 ± 7
21.1	Strongly zoned	829	792	229	0.29	0.008	0.4087 ± 5	0.0746 ± 3	0.2110 ± 25	0.8194 ± 89	3869 ± 42	3858 ± 32	3941 ± 2
1.6	Strongly zoned	955	814	429	0.53	0.005	0.4290 ± 12	0.1330 ± 3	0.2202 ± 26	0.8727 ± 96	4023 ± 42	4045 ± 33	4014 ± 4
1.8	Strongly zoned	886	832	226	0.27	0.002	0.4205 ± 8	0.0691 ± 4	0.2110 ± 30	0.8298 ± 98	3869 ± 50	3895 ± 35	3984 ± 3
1.5	Strongly zoned	969	857	256	0.30	0.001	0.4329 ± 10	0.0754 ± 2	0.2201 ± 25	0.8713 ± 93	4021 ± 42	4039 ± 32	4028 ± 3
20.1	Strongly zoned	897	911	259	0.28	0.001	0.3820 ± 7	0.0731 ± 2	0.2020 ± 24	0.7864 ± 85	3719 ± 40	3740 ± 31	3840 ± 3
13.2	Strongly zoned	984	968	402	0.42	0.009	0.4053 ± 5	0.1017 ± 3	0.1917 ± 23	0.7836 ± 88	3545 ± 39	3730 ± 32	3929 ± 2
11.4	Strongly zoned	1114	1035	336	0.32	0.032	0.4257 ± 6	0.0837 ± 3	0.2137 ± 24	0.8285 ± 88	3915 ± 41	3890 ± 31	4002 ± 2
4.3	Strongly zoned	1092	1039	308	0.30	0.007	0.4168 ± 12	0.0756 ± 2	0.2091 ± 25	0.8184 ± 89	3838 ± 41	3855 ± 32	3971 ± 4
27.1	Strongly zoned	1131	1088	321	0.30	0.034	0.3941 ± 8	0.0758 ± 4	0.2109 ± 26	0.8213 ± 91	3867 ± 44	3865 ± 32	3887 ± 3
13.1	Strongly zoned	1335	1247	624	0.50	0.003	0.4207 ± 9	0.1263 ± 6	0.2031 ± 26	0.8040 ± 93	3737 ± 44	3804 ± 33	3985 ± 3
34.2	Strongly zoned	953	1666	711	0.43	0.081	0.3058 ± 10	0.1092 ± 3	0.1202 ± 13	0.4696 ± 49	2295 ± 24	2482 ± 22	3500 ± 5
17.2	Mottled	790	868	127	0.15	0.009	0.3869 ± 13	0.0373 ± 4	0.1899 ± 33	0.7433 ± 90	3514 ± 55	3583 ± 33	3859 ± 5
14.2	Mottled	1067	1254	90	0.07	0.027	0.3601 ± 28	0.0188 ± 2	0.1879 ± 29	0.7172 ± 77	3480 ± 50	3486 ± 29	3750 ± 12
6.2	Mottled	1484	1665	130	0.08	0.092	0.3783 ± 10	0.0206 ± 3	0.1948 ± 34	0.7405 ± 81	3597 ± 58	3572 ± 30	3825 ± 4
22.1	Mottled	1212	1724	48	0.03	0.022	0.3328 ± 8	0.0073 ± 2	0.1595 ± 39	0.6097 ± 67	2991 ± 68	3069 ± 27	3630 ± 4
34.1	Mottled	1533	2851	1195	0.42	0.247	0.2855 ± 4	0.1145 ± 3	0.1219 ± 16	0.4462 ± 54	2325 ± 29	2378 ± 24	3393 ± 2
2.1	Mantle	87	79	86	1.09	0.031	0.3518 ± 34	0.2822 ± 53	0.2029 ± 64	0.7810 ± 174	3734 ± 108	3721 ± 63	3715 ± 15
34.3	Mantle	109	94	126	1.34	0.012	0.3562 ± 24	0.3540 ± 26	0.2070 ± 43	0.7858 ± 138	3803 ± 72	3738 ± 50	3734 ± 10
5.1	Mantle	113	105	125	1.18	0.033	0.3500 ± 35	0.3140 ± 24	0.1985 ± 40	0.7489 ± 123	3660 ± 67	3603 ± 46	3707 ± 15
17.1	Mantle	92	110	61	0.56	0.071	0.3444 ± 25	0.1448 ± 13	0.1692 ± 33	0.6509 ± 100	3161 ± 57	3232 ± 39	3682 ± 11
30.1	Mantle	142	148	84	0.57	0.062	0.3451 ± 27	0.1488 ± 10	0.1949 ± 32	0.7483 ± 104	3599 ± 55	3601 ± 38	3685 ± 12

6.1	Mantle	168	148	167	1.13	0.006	0.3641 ± 25	0.2878 ± 29	0.2034 ± 41	0.7974 ± 129	3742 ± 70	3780 ± 47	3767 ± 11
14.1	Mantle	161	165	81	0.49	0.012	0.3407 ± 34	0.1305 ± 16	0.2039 ± 44	0.7712 ± 122	3750 ± 73	3685 ± 45	3666 ± 15
18.1	Mantle	201	180	201	1.12	0.001	0.3604 ± 15	0.2925 ± 18	0.2052 ± 34	0.7870 ± 111	3773 ± 56	3742 ± 40	3752 ± 6
Table 1 (continued)													
16.1	Mantle	226	202	220	1.09	0.046	0.3627 ± 12	0.2888 ± 11	0.2083 ± 34	0.7843 ± 113	3825 ± 58	3733 ± 41	3761 ± 5
31.1	Recrystallized	137	133	95	0.71	0.005	0.3608 ± 12	0.1882 ± 10	0.2037 ± 33	0.7725 ± 108	3748 ± 55	3690 ± 39	3753 ± 5
1.7	Recrystallized	128	134	26	0.19	0.139	0.3835 ± 29	0.0541 ± 11	0.2170 ± 56	0.7717 ± 116	3969 ± 94	3687 ± 42	3846 ± 11
1.1	Recrystallized	148	144	23	0.16	0.012	0.4244 ± 59	0.0410 ± 15	0.2090 ± 87	0.8166 ± 130	3836 ± 145	3848 ± 46	3998 ± 21
11.2	Recrystallized	159	156	30	0.19	0.008	0.4039 ± 62	0.0491 ± 7	0.2088 ± 48	0.8136 ± 133	3833 ± 81	3838 ± 47	3924 ± 23
19.1	Recrystallized	198	173	198	1.14	0.012	0.3665 ± 18	0.2976 ± 19	0.2069 ± 36	0.7955 ± 118	3801 ± 61	3773 ± 43	3777 ± 8
25.1	Recrystallized	210	178	211	1.18	0.012	0.3608 ± 18	0.3103 ± 18	0.2147 ± 33	0.8192 ± 108	3931 ± 55	3857 ± 38	3753 ± 5
32.1	Recrystallized	202	180	220	1.22	0.157	0.3562 ± 12	0.3250 ± 12	0.2054 ± 31	0.7734 ± 106	3775 ± 52	3693 ± 39	3734 ± 5
3.2	Recrystallized	207	196	49	0.25	0.065	0.4170 ± 35	0.0637 ± 15	0.2126 ± 69	0.8304 ± 174	3896 ± 114	3897 ± 62	3971 ± 13
28.1	Recrystallized	265	232	265	1.14	0.001	0.3619 ± 13	0.2963 ± 10	0.2068 ± 33	0.7987 ± 113	3798 ± 56	3784 ± 41	3758 ± 5
9.1	Recrystallized	310	256	433	1.69	0.015	0.3571 ± 16	0.4372 ± 20	0.2026 ± 36	0.7828 ± 125	3730 ± 61	3727 ± 45	3738 ± 7
29.1	Recrystallized	305	273	390	1.43	0.712	0.3396 ± 9	0.3796 ± 20	0.2003 ± 27	0.7528 ± 91	3691 ± 46	3618 ± 33	3661 ± 4
23.1	Recrystallized	336	397	64	0.16	0.012	0.3217 ± 13	0.0421 ± 12	0.1880 ± 58	0.7208 ± 87	3482 ± 99	3499 ± 33	3578 ± 6

[a] Radiogenic Pb, corrected for common Pb using ^{204}Pb and, except for large corrections, Broken Hill Pb composition (see text)
[b] Percentage of total ^{206}Pb which is common

Fig. 3 A Concordia plot of zircon U-Pb analyses from tonalitic gneiss SAB91-63. Most of the analyses define a branched array; the less altered zircon shows only minor recent isotopic disturbance (constant radiogenic ^{207}Pb/^{206}Pb), the more altered zircon shows in addition the effects of ancient Pb loss. Two analyses of the core of grain 15 plot well above the main group, analyses of overgrowths plot well below. Analytical uncertainties 1σ. **B** Concordia plot of zircon U-Pb analyses from tonalitic gneiss SAB91-37. The older cluster consists of data from crystal centres, the younger of data from overgrowths, recrystallized areas and zoned intermediate layers (see text). The different types of zircon show the effects of at least two post-3.6 Ga episodes of isotopic disturbance. Analytical uncertainties 1σ. **C** Concordia plot of zircon U-Pb analyses from tonalitic gneiss SAB94-134. The older cluster contains only analyses of crystal centers, which define a branched array, reflecting different responses to post-crystallization isotopic disturbance. The cluster contains some analyses of recrystallized zircon (cf. Fig. 2E), but not of the recrystallized zircon with high Th/U (>1), which plots with the analyses of mantles in a separate cluster below

3.6 Ga. Many other analyses are strongly discordant. Distribution of the data is very closely related to the type of zircon analyzed. The older cluster is composed only of

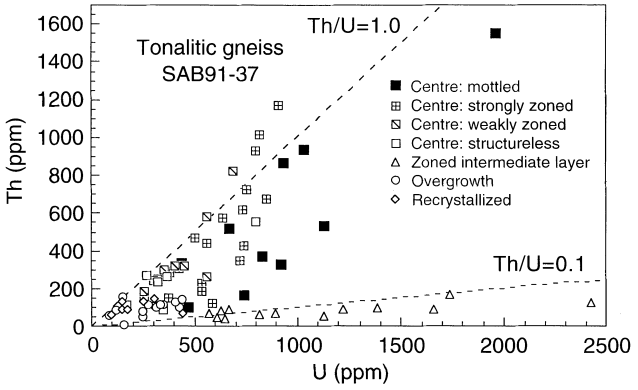

Fig. 4 U and Th contents of different zircon types from tonalitic gneiss SAB91-37. Note in particular the correlation between strength of zoning and Th and U content in the crystal centers, and the consistently low Th content of the younger overgrowths, recrystallized areas and intermediate layers

analyses of centers that are unzoned or weakly zoned. Analyses of strongly zoned and mottled centers mostly are more discordant. In contrast, the younger cluster consists of analyses of overgrowths, intermediate layers and recrystallized areas. Overgrowth analyses generally are near concordant, but analyses of the intermediate layers show a wide range of discordance.

A first order interpretation of the data is relatively straightforward – the bulk of the zircon population, represented by the grain centers, crystallized at about 4.0 Ga. At about 3.6 Ga more zircon grew, first as a structurally complex zoned layer and then as a relatively structureless overgrowth. At about the same time, some of the pre-existing zircon was recrystallized. The interpretation of the ages of zircon growth is more difficult than for SAB91-63, where a branched data distribution was clearly evident, but the same interpretation principle can be applied. If one assumes that, as the distribution of analyses implies, isotopic disturbance (probably Pb loss) leads to a reduction in radiogenic $^{207}Pb/^{206}Pb$, then a *minimum* age for the older zircon can be calculated from the weighted mean of the group of highest radiogenic $^{207}Pb/^{206}Pb$ values that are equal (based on a test of the variance ratio F between observed and expected standard errors of the mean) within analytical uncertainty. Eleven analyses from eight centers, ranging from structureless to strongly zoned, satisfy this criterion. Their weighted mean radiogenic $^{207}Pb/^{206}Pb$, 0.4285 ± 0.0007 (1σ), is equivalent to an age of 4012 ± 6 Ma (tσ).

Unlike the SAB91-63 data, the remaining analyses in the cluster do not form a linear array, but disperse in a broad band towards lower $^{207}Pb/^{206}Pb$ and $^{206}Pb/^{238}U$. However, 23 of the 31 analyses in the group define a straight line (MSWD = 1.06) with concordia intersections of 4026 ± 10 Ma (tσ) and 1182 +265/−305 Ma (tσ). The remainder are collinear (MSWD = 0.20) with three highly discordant analyses of mottled zircon, defining a line with concordia intercepts of 4001 ± 20 Ma (tσ) and 1842 +165/−185 Ma (tσ). All three older ages are equal within analytical uncertainty, consistent with the evidence from zircon structures that all analyses sample the same zircon growth generation. The best interpretation of the data is that the zircons are at least 4012 ± 6 Ma.

The analyses of overgrowths can be treated similarly, but only 7 of the 13 measurements in the younger cluster are equal within analytical uncertainty at the highest radiogenic $^{207}Pb/^{206}Pb$. The weighted mean value of 0.3220 ± 0.0013 (1σ) is equivalent to an age of 3579 ± 15 Ma (tσ). On the other hand, all the overgrowth data are well fitted (MSWD = 1.08) to a transverse linear array with concordia intersections of 3655 +110/−65 Ma (tσ) and 2307 +405/−795 Ma (tσ). This coincides very closely with the line defined by the widely dispersed analyses of the intermediate layers (MSWD = 1.33), which has concordia intersections of 3623 ± 18 Ma (tσ) and 1706 +65/−70 Ma (tσ), strongly suggesting that the intermediate layers and overgrowths formed at virtually the same time and suffered the same Pb-loss history. If the two data sets are therefore combined (MSWD = 1.39), the concordia intersections of the array become 3611 ± 11 Ma (tσ) and 1692 +55/−60 Ma (tσ), providing the best estimate of the crystallization age of these zircon types.

Most analyses of recrystallized areas also fall on a well-defined (MSWD = 0.45) linear array emanating from the younger cluster (the exception being 38.1), but a different array from that of the overgrowth and intermediate layer data. A similar upper intersection to the latter (3604 ± 20 Ma (tσ)) indicates recrystallization approximately coincident with the formation of the intermediate layers and overgrowths, but a younger lower intercept of 844 +250/−290 Ma (tσ) indicates a different Pb-loss history. In this context, it is of interest to note the similarity of the, admittedly rather poorly defined, pairs of lower intersection ages from the two main zircon groups, 1842 +165/−185 and 1182 +265/−305 Ma from the older group, 1692 +55/−60 and 844 +250/−290 Ma from the younger. Three of the six analyses in the cluster at about 3.75 Ga come from one grain (grain 8). It is likely, therefore, that the cluster is not just a chance consequence of Pb loss from older zircon, but records another thermal event in the rock's history.

Although the zircons in this sample are extremely complex, petrographic differentiation of the various growth morphologies allows resolution of the age of the rock (4012 ± 6 Ma), the principal metamorphism (3611 ± 11 Ma), and other events that affected the zircon U-Pb systems (~3.75 Ga, ~1.7 Ga and ~1.0 Ga).

Granodioritic gneiss SAB94-134

The zircons from sample SAB94-134 are similar to those in the other two samples, consisting mostly of large (up to 300 μm diameter), subhedral grains, many of which have turbid centers. However, important differences include the prevalence (~25% of the population) of pris-

matic grains (aspect ratios mostly 3 to 5) and of grains that are either clear, or mostly clear when examined in transmitted light. Except for the more turbid areas, inclusions and intense microfracturing are relatively rare. HF etching reveals that the internal structure of the grains is generally much simpler than in the other samples, although some grains have complex, mottled centers, the majority (~80%) show relatively simple, concentric, euhedral growth zoning (Fig. 2E) reminiscent of that reported by Bowring et al. (1989) in zircon from the nearby sample of granitic gneiss, SP405.

An unusual feature of the zircons is the wide variation in the strength of zoning from grain to grain, and particularly within grains. Some grains have strong zoning throughout; in others the zoning is barely visible. Some grains have the strongest zoning near the middle, others the weakest. Some grains are strongly zoned at one end and not at the other (Fig. 2F), and/or contain patches of very weak zonation within zircon that is strongly zoned. Surrounding virtually all grains is an outermost layer of unzoned or very weakly zoned zircon that, like the similarly structured areas in the crystal centers, is resistant to the HF etch. The presence of structurally continuous residual 'ghost zoning' in the etch-resistant areas suggests that these are regions of in-situ recrystallization (cf. Black et al. 1986), not areas of new zircon growth. It is therefore more appropriate to describe the structureless or very weakly zoned outermost layers of these zircons as mantles, not overgrowths. Cathodoluminescence imaging shows the presence of some very thin (most <15 μm), structurally transgressive outer layers that probably are true overgrowths, but none was thick enough to analyze.

Sixty three analyses from 32 grains are listed in Table 1. The coherence between zircon type and composition is particularly strong. For example, most of the zoned zircon has very similar Th/U (~0.3), with the U and Th contents increasing with the strength of the zoning. The few mottled centers sampled are mostly characterized by high U (>850 ppm), and much lower Th (≤ 130 ppm). Mantles and recrystallized areas are consistently low in U, but show a distinct bimodality in Th/U; approximately half the analyses have Th/U similar to the zoned zircon while the remainder have ratios greater than 1.1.

These differences in zircon type and chemical composition carry over into differences in isotopic composition. On a concordia diagram (Fig. 3C) the analyses form two clusters, one near 4.0 Ga and the other near 3.75 Ga. The upper cluster contains only analyses of grain centers, with several analyses of areas with weak zoning being concordant within analytical uncertainty. Analyses of areas with strong zonation tend to be more discordant, and analyses of most of the mottled centers are yet more discordant, but fall on the same trend. Several analyses of recrystallized areas plot within the same cluster, but none of those are recrystallized areas with high Th/U. Data in the lower cluster include all analyses of mantles, plus all analyses of recrystallized areas with high Th/U. Where recrystallization has altered the zircon's chemical composition (raised Th/U by Th gain and/or U loss), it also has reset the isotopic composition through loss of radiogenic Pb. Some large discrepancies between $^{206}Pb/^{238}U$ and $^{208}Pb/^{232}Th$ apparent ages in the recrystallised zircon from SAB91-37 (Table 1) suggest that this process does not always go to completion, or elemental mobilisation can be selective.

The analyses in the lower cluster are dispersed in a relatively poorly defined array, interpretation of which is complicated by many of the data lying within analytical uncertainty of concordia but having significant differences in radiogenic $^{207}Pb/^{206}Pb$. The best estimate of the minimum age of the high Th/U mantles and high Th/U recrystallization is obtained from the group of seven analyses with highest $^{207}Pb/^{206}Pb$, the weighted mean of which (0.3619 ± 0.0005 (1σ)) is equivalent to an age of 3758 ± 5 Ma ($t\sigma$). The transverse discordance array is not well enough defined to provide an alternate age estimate by linear regression, but in contrast, the three analyses of low Th/U mantles have an equal $^{207}Pb/^{206}Pb$ of 0.3439 ± 0.0016 (1σ), equivalent to an age of 3680 ± 31 Ma ($t\sigma$), significantly younger.

Within the upper cluster, eight analyses from four grains are equal within analytical uncertainty at the highest measured radiogenic $^{207}Pb/^{206}Pb$ (MSWD = 0.86). The weighted mean value, 0.4339 ± 0.0004 (1σ), is equivalent to an age of 4031 ± 3 Ma ($t\sigma$), which is a minimum age for the crystallization of the zoned zircon. As in the other two samples the discordance array is branched, with most analyses dispersed along a transverse trend. Defining this trend by regression analysis is complicated by the relatively large amount of scatter, probably due to isotopic disturbance during the ~3.75 Ga event. Best definition of the trend is provided by some multiple analyses within single grains. For example, the eight analyses from grain 1 (3 weakly zoned, 3 strongly zoned and 2 recrystallized) fit within analytical uncertainty (MSWD = 1.11) to a line with concordia intersections of $4026 +17/-12$ and $2616 +390/-510$ Ma ($t\sigma$), the five analyses of grain 3 (4 weakly zoned, 1 recrystallized) fit within analytical uncertainty (MSWD = 0.16) to the same line (intersections $4017 +43/-17$ and $2042 +2015/-1960$ Ma ($t\sigma$)), as do the five analyses of grain 7 (all weakly zoned, MSWD = 0.53), with concordia intersections of $4016 +60/-16$ and $2667 +1410/-1330$ Ma ($t\sigma$). Combining the data for these three grains defines a line (MSWD = 0.63) with concordia intersections of $4023 +10/-8$ and $2597 +305/-370$ Ma ($t\sigma$), along which many of the analyses from other grains fall (Fig. 3C). This upper intersection age is the same within uncertainty as the mean highest $^{207}Pb/^{206}Pb$ age, 4031 ± 3 Ma which we interpret as the age of the igneous event which formed this rock.

Implications of the zircon data

There is unequivocal evidence in each of the samples discussed above for a major component of the zircon population being ≥4.0 Ga old. A crucial question to be considered, however, is whether that component records the 'age' of the rock. Geochronology has now developed to the extent that the concept of a rock's age is no longer a simple one, particularly in polymetamorphic terranes. It is quite feasible, for example, to find in the zircon from a polymetamorphosed orthogneiss an isotopic record of two or more episodes of metamorphism, the magmatic event, and the components of the protolith from which the magma was derived. This is a consequence of the chemical stability of zircon under a wide range of igneous and metamorphic conditions, and the fact that the zircon U-Pb closure temperature (> 900 °C) exceeds the maximum temperature reached in many igneous and metamorphic systems (Lee et al. 1997).

In such circumstances, the concept of the 'age' of a rock becomes a matter of definition and sometimes confusion. For example, Moorbath et al. (1997), in their discussion of Nd isotopic data from early Archean rocks, concluded that '...it is probable that the age of the Acasta gneisses is only ~3.37 Ga, although both the zircon U-Pb ages ...and the initial ε_{Nd} ...provide incontrovertible evidence for the existence of a substantially older precursor ...which is well worth searching for in the field...' (p. 222). Moorbath and his colleagues arrived at this conclusion by assuming that the linear array defined by the whole-rock isotopic compositions of these polymetamorphic rocks on a Sm-Nd isotope correlation diagram can be used to calculate an age of geological significance, namely that of the main metamorphism and formation of the gneissic fabric. By construing the 'age' of the gneisses to be the age of the '...event that produced the Acasta gneisses as we now see them ...' (p. 228) and interpreting the ~4.0 Ga zircon that they contain to be inherited, Moorbath and others overlooked the fact that the Acasta gneisses are orthogneisses, namely deformed igneous rocks. The ancient precursors to the gneisses do not need to be searched for – they are, although now in a deformed state, the gneisses themselves. The geological significance of the date that corresponds to the slope of the linear array published by Moorbath is unclear (e.g. Bowring and Housh 1996).

We prefer to define the age of an orthogneiss as being the age of crystallization of the igneous rock which is its undeformed equivalent. By this definition, the ages of magmatic events are recognized independently of the timing of subsequent episodes of deformation. To establish the ages of the three samples discussed in the present paper, it is therefore necessary to establish which of the dated zircon generations crystallized from a magma.

Sample SAB91-63 is the most straightforward; with the exception of clearly recognizable overgrowths and one core, all the analyzed zircon is the same age, 4002 ± 4 Ma. By analogy with orthogneisses elsewhere we interpret most of the zircon to have crystallized from a magma, the one identified zircon core to be a remnant of an older component within that magma, and the overgrowths to be the product of later metamorphism. This interpretation is strongly supported by the fact that much of the analyzed zircon shows the fine euhedral growth zoning common in zircon from granitic rocks, and the younger overgrowths show the lack of zoning and very low Th/U common in zircon produced by high grade metamorphism (e.g. Williams and Claesson 1987). Orthogneiss SAB91-63 is therefore interpreted as a 4002 ± 4 Ma tonalite which incorporated a small amount of material at least 4065 Ma old, and was metamorphosed ~3.73 Ga ago.

The data and zircons from SAB91-37 are more complex, but a similar line of reasoning can be followed. The main reason for the increased complexity is that the zircon records a more complex post-magmatic history. The centers of the SAB91-37 zircons closely resemble the igneous zircon from SAB91-63; within a matrix of strongly altered zircon are preserved patches of euhedrally zoned zircon, nearly all of which have an isotopic composition indicating the same age, 4012 ± 6 Ma. We interpret this to be the age of tonalite crystallization. Surrounding those centers is a composite layer of zircon consisting in part of multiple crystallites subsequently overgrown by strongly zoned zircon with a much simpler crystal form. This layer is much younger, 3611 ± 11 Ma, and has the very low Th/U commonly found in metamorphic zircon. The unusual crystallites and presence of zoning suggest that the metamorphism involved the production of partial melt, a conclusion consistent with the presence nearby of ~3.6 Ga granites (Williams et al. 1991). The composite layer is in turn overgrown by structureless, low-U zircon of the same age, marking a later stage of the metamorphic event. Also coincident with the metamorphism is local recrystallization of some of the pre-existing igneous zircon. The patterns of Pb loss from all zircon types, especially the composite metamorphic layer, indicate a later event at 1.69 ± 0.06 Ga. Although some ^{40}Ar-^{39}Ar cooling dates for biotite and muscovite (Bowring et al. 1997; unpublished data) are as young as 1.7 Ga, there is no known thermal event of this age.

Although the zircon and data from the granodioritic gneiss SAB94-134 are similarly complex, interpretation of the analyses is made simpler by the better preservation of the zircon growth structures; mottled zircon is relatively rare. The zircon population is dominated by very simply structured, finely euhedrally zoned zircon, all of which has the same Th/U and same age, 4031 ± 3 Ma. This we interpret as the crystallization age of the granodiorite. The zircon clearly has been affected by metamorphism, which for the most part caused widespread recrystallization, isotopic resetting and, in some areas, enhancement of Th/U rather than the development of simple overgrowths. The metamorphism

occurred at 3758 ± 5 Ma, which is very similar to the ages of ~3.73 and ~3.75 Ga obtained on a few of the zircons from SAB91-63 and SAB91-37 respectively, implying that those samples also were affected by the same event.

The ~3.75 Ga event probably accounts for much of the dispersion in radiogenic $^{207}Pb/^{206}Pb$ reported in previously analyzed Acasta zircon by Bowring et al. (1989), and the 3.61 Ga metamorphism that affected SAB91-37 coincides very closely with the ~3.6 Ga age of structureless zircon found in both previously analyzed samples. In none of the present samples do we find evidence for metamorphism at ~3.37 Ga that might account for the regional Nd whole-rock 'isochron' reported by Moorbath et al. (1997), although we have found local metamorphic zircon growth between 3.1 and 3.4 Ga in the area (Williams et al. 1991), and Stern et al. (1997) and Bowring (unpublished data) have reported 3.4 Ma granite sheets and leucosomes in the same region.

The bottom line is that careful ion-probe geochronology can be used to determine a complex chronology of igneous and metamorphic events in complex Archean gneisses. In particular, protolith ages can be recovered with careful work, once the zircons have been characterized. A thorough understanding of the relationship between U-Pb dates and zircon texture is required.

These interpretations show that the definition of 'age' in rocks such as the Acasta gneisses is not merely a matter of semantics – Moorbath et al. (1997) were led by their particular definition to conclude that a ~4.0 Ga protolith for the gneisses has yet to be found, whereas we argue instead that the Acasta gneisses themselves are actually preserved remnants, possibly chemically intact, of the only known terrestrial Priscoan magmas, vital clues to the composition and genesis of some of the Earth's earliest differentiated crust. Samples of Acasta gneiss that are 3.96 Ga and older range in compositon from granite to tonalite and contain cores of even older zircon. Geochemically, the Acasta gneisses are similar to other Archean gneiss complexes and are not unusual in any way (Bowring et al. 1990; Housh and Bowring 1993). The presence of inherited zircon cores as old as 4.06 Ga and the range in whole rock initial ε_{Nd} (+4 to −4) (Bowring and Housh 1995) suggests that the parental magmas were formed by interaction of mantle-derived melts with pre-existing zircon-bearing crust and imply that even older Acasta gneisses await discovery.

Acknowledgements This work was supported by NSF(EAR). Field work in the Acasta gneisses was possible through the encouragement and generosity of Bill Padgham in yellow knife John Mga and Shane Paxton prepared the Zircons and Neil Gabbitas provided assistance with the photoplate.

References

Armstrong RL (1991) The persistant myth of crustal growth. Aust J Earth Sci 38: 613–30

Black LP, Williams IS, Compston W (1986) Four zircon ages from one rock: the history of a 3930 Ma-old granulite from Mount Sones, Enderby Land, Antarctica. Contrib Mineral Petrol 94: 427–437

Bowring SA, Housh TB (1995) Earth's early evolution. Science 269: 1535–1540

Bowring SA, Housh TB (1996) Response to technical comment: Sm- Nd Isotopic data and Earth's evolution. Science 273: 1878–1879

Bowring SA, Williams IS, Compston W (1989) 3.96 Ga gneisses from the Slave Province, Northwest Territories, Canada. Geology 17: 971–975

Bowring SA, Housh TB, Isachsen CE (1990) The Acasta gneisses: remnant of Earth's early crust. In: Newsom HE, Jones JH (eds) Origin of the Earth. Oxford Univ Press, Oxford, pp 319–343

Bowring SA, Housh TB, Hildebrand RS, Isachsen CE, Coleman DS, Northrup CJ, Grove TL, Collerson KD (1997) An overview of the geologic framework of the Acasta Gneisses (abstract). Geol Assoc Can Abstr Prog 22: A16

Bridgewater D, Schiotte L (1991) The Archean gneiss complex of northern Labrador: a review of current results, ideas, and problems. Bull Geol Soc Den 39: 153–166

Collerson KD, Campbell LM, Weaver BL, Palacz ZA (1991) Evidence for extreme mantle fractionation in early Archaean ultramafic rocks from northern Labrador. Nature 349: 209–214

Compston W, Pidgeon RT (1986) Jack Hills, a further occurence of very old detrital zircons in Western Australia. Nature 321: 766–769

Davidek K, Martin MW, Bowring SA, Williams IS (1997) Conventional U-Pb geochronology of the Acasta gneisses using single crystal zircon fragmentation technique (abstract). Geol Assoc Can Abstr Prog 22: A35

Froude DO, Ireland TR, Kinny PD, Williams IS, Compston W, Williams IR, Myers JS (1983) Ion microprobe identification of 4,100–4,200 Myr-old terrestrial zircons. Nature 304: 616–618

Goldich SS, Mudrey MG (1972) Dilatancy model for discordant U-Pb zircon ages. In: Tugarinov(ed) Contributions to recent geochemistry and analytical chemistry. Nauka Publ. Office, Moscow, pp 415–418

Lee JKW, Williams IS, Ellis DJ (1997) Pb, U and Th diffusion in natural zircon. Nature 390: 159–161

Harland WB, Armstrong RL, Cox AV, Craig LE, Smith AG, Smith DG (1990) A Geologic Time Scale 1989. Cambridge University Press, Cambridge UK

Housh T, Bowring SA (1993) Geochemical constraints on the formation of the Earth's oldest extant crust (abstract). Geol Soc Am Abstr Prog 25 (6): A-73

McCulloch M, Bennett VC (1994) Progressive growth of the Earth's continental crust and depleted mantle: geochemical constraints. Geochim Cosmochim Acta 58: 4717–4738

Moorbath S, Whitehouse MJ, Kamber BS (1997) Extreme Nd-isotope heterogeneity in the early Archaean; fact or fiction? Case histories from northern Canada and WestGreenland. Chem Geol 135: 213–231

Mueller PA, Wooden JL, Nutman AP (1992) 3.96 Ga zircons from an Archean quartzite, Beartooth Mountains, Montana. Geology 20: 327–330

Nutman AP, McGregor VR, Friend CRL, Bennett VC, Kinny PD (1996) The Itsaq Gneiss Complex of southern West Greenland; the world's most extensive record of early crustal evolution (3900–3600 Ma). Precambrian Res 78: 1–39

Pidgeon RT (1992) Recrystallization of oscillatory zoned zircon: some geochronological and petrological implications. Contrib Mineral Petrol 110: 463–472

Song B, Nutman AP, Liu D, Wu J (1996) 3800–2500 Ma crustal evolution in the Anshan area of Liaoning Province, northeastern China. Precambrian Res 78: 79–94

Steiger R, Jager E (1977) Subcommission on geochronology: convention on use of decay constants in geo- and cosmochronology. Earth Planet Sci Lett 36: 359–362

Stern RS, Bleeker W, Theriault, RJ (1997) U-Pb SHRIMP zircon chronology of 4.02 Ga tonalite, Acasta Gneiss Complex, Canada (abstract). Geol Assoc Can Abstr Prog 22: A142

Taylor SR, (1992) Solar system evolution. Cambridge University Press, Cambridge UK

Tera F, Wasserburg GJ (1974) U-Th-Pb systematics on lunar rocks and inferences about lunar evolution and the age of the Moon. Proc 5th Lunar Sci Conf (Suppl 5), Geochim Cosmochim Acta 2: 1571–99

Wetherill GW (1956) An interpretation of the Rhodesia and Witswatersrand age patterns. Geochim Cosmochim Acta 9: 290–292

Note added in proof: Stern and Bleeker (1998) have recently reported a revised age of 4025 +/−15 Ma for their Acasta gneiss sample BNB95-103, collected from near one of the Bowring et al. (1989) localities (Stern et al., 1997), consistent with the Acasta gneiss ages up to 4031 +/− 3 Ma reported here.

Stern, R.A. and Bleeker, W. 1998. Age of the world's oldest rocks refined using Canada's SHRIMP: The Acasta Gneiss Complex, Northwest Territories, Canada Geoscience Canada: 25: 27–31

Williams IS, Claesson S (1987) Isotopic evidence for the Precambrian provenance and Caledonian metamorphism of high grade paragneisses from the Seve Nappes, Scandinavian Caledonides: II. Ion-microprobe zircon U-Th-Pb. Contrib Mineral Petrol 97: 205–217

Williams IS, Bowring SA, Compston W, Housh T, Isachsen CE (1991) Improved definition of the areal extent and lithological diversity of the oldest-known terrestrial rocks, NWT, Canada (abstract). Geol Assoc Can Abstr Prog 16: A132

Williams IS, Buick I, Cartwright I (1996) An extended episode of early Mesoproterozoic metamorphic fluid flow in the Reynolds Range, central Australia. J Metamorphic Geol 14: 29–47